Global NEST Journal, Vol 25, No 4, pp 86-94

MTBE adsorption on surface modified adsorbent kaolin-KOH – A study on kinetic equilibrium and surface morphology

Mahendran S.[1], Packialakshmi S.[2], Al-Zaqri N.[3]*, Boshaala A.[4,5], Krishnapriya S.[6], Senthil Kumar M.[7], Gokulan R.[8]*

[1]Department of Civil Engineering, PSNA College of Engineering and Technology, Dindigul – 624 622, Tamil Nadu, India
[2]Department of Civil Engineering, Sathyabama Institute of Science and Technology, Chennai 600 119, Tamil Nadu, India
[3]Department of Chemistry, College of Science, King Saud University, P.O. Box- 2455, Riyadh 11451, Saudi Arabia
[4]Research Centre, Manchester Salt & Catalysis, Unit C, 88-90 Chorlton Rd, M154AN Manchester, United Kingdom
[5]Libyan Authority for Scientific Research, P.O. Box 80045, Tripoli, Libya
[6]Department of Civil Engineering, AAA College of Engineering and Technology, Sivakasi – 626 123, Tamil Nadu, India
[7]Department of Environmental Engineering, College of Engineering and Technology, Bule Hora University, Bule Hora, West Guji, Ethiopia
[8]Department of Civil Engineering, GMR Institute of Technology, Rajam – 532 127, Andhra Pradesh, India
Received: 20/12/2022, Accepted: 06/01/2023, Available online: 09/01/2023
*to whom all correspondence should be addressed: e-mail: nalzaqri@ksu.edu.sa, gokulan.r@gmrit.edu.in, gokulravi4455@gmail.com
https://doi.org/10.30955/gnj.004663

Graphical abstract

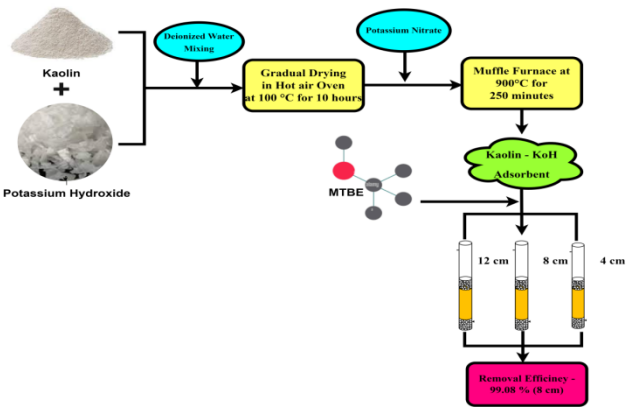

Abstract

The purpose of this research was to evaluate the effectiveness of low-cost adsorbents for the removal of MTBE by employing natural kaolin clay with surface modification by KOH. The feasibility of MTBE examination by High Pressure Liquid Chromatography (HPLC) in aqueous solution was investigated. To get rid of impurities, the kaolin clay goes through a beneficiated process. Then, the thermal procedure was carried out at 990°C to prepare the adsorbent. XRD, SEM, and FTIR were used to characterize the geochemical and surface characteristics of the kaolin adsorbent. Basic operation parameters were evaluated in the batch experiment, including beginning MTBE concentrations, pH, contact time, and adsorbent dosage. For three different sized columns that were 12cm, 8cm, and 4cm, respectively, the percentage removal efficiency for MTBE was recorded as 97.79%, 99.08%, and 98.13%. This study demonstrated that the adsorbent's contact time and retention period are crucial for the elimination of MTBE, as demonstrated by the Thomas model and Thomson model with R^2 values of 97.81, 99.21, and 98.36.

Keywords. MTBE, surface modification, adsorption, thermal process, kinetic study

1. Introduction

Methanol and isobutylene react chemically to produce MTBE (Methyl Tertiary-Butyl Ether), a chemical substance. MTBE is almost solely utilized as a fuel additive in motor gasoline and is produced in extremely huge amounts (Attarian and Mokhtarani, 2021). It belongs to a class of substances called "oxygenates" since it increases the oxygen content of gasoline. It is a flammable, colourless liquid that has been added to unleaded gasoline at room temperature (Ma *et al.*, 2021). It raises the octane and oxygen content of gasoline while also lowering pollutant emissions. This causes groundwater contamination and a decline in the quality of the water (Zhi and Liu, 2016). Additionally, it is employed in small doses as a laboratory solvent and in a few medical procedures. Some water sources contain MTBE, mainly in metropolitan areas where underground gasoline storage tanks are leaking (Gong *et al.*, 2016). This combustible substance has been found in the air surrounding some fuel facilities, in cities where MTBE is still used in gasoline, and when people are filling up their cars at gas stations (Attarian and Mokhtarani, 2021). The US Environmental Protection Agency (EPA) has determined that MTBE is a possible human carcinogen at high doses and that MTBE levels in drinking water should be kept below 20–40 mg/L (Ren *et al.*, 2021). By inhaling contaminated air and consuming contaminated water, people might be exposed to MTBE. MTBE production, transportation, and gasoline treatment may expose workers to higher exposure levels (Zhang *et al.*, 2019). This MTBE is classified as a carcinogenic substance. Acute health consequences are not anticipated

to be caused by regular exposure to MTBE in drinking water, but inhalation exposure to the chemical increased the risk of liver, kidney, and testicular tumours (Amanollahi *et al.*, 2019). Humans that received MTBE orally developed leukaemia and lymphoma. MTBE was removed from an aqueous solution using a variety of techniques, including filtering, electrodialysis, adsorption, and photocatalysis (Park *et al.*, 2019). In this case, MTBE removal from aqueous phase solutions has been highlighted as a possible application for adsorption technology. Adsorption techniques do not introduce unwanted by-products into drinking water, although if surface-modified adsorbent is used to adsorb MTBE, significant adsorbent utilization rates can be anticipated (Yang *et al.*, 2019). To adsorb small particles, molecules, or ions from a solution, many types of adsorbents can be made from various basic materials (Yunhui *et al.*, 2018). $Al_2Si_2O_5(OH)_4$ is the main component of the clay mineral kaolin, which has been extensively exploited in a wide range of technical applications (Jiang *et al.*, 2018). Because it offers an affordable, environmentally benign, and abundant alternative, kaolin clay is a potential adsorbent (Masle *et al.*, 2018). The adsorption of MTBE from aqueous solution onto the surface-modified Kaolin adsorbent was examined in the current study. The adsorbent was made by KOH chemical using a high temperature technique (Muller *et al.*, 2018). The use of columns of various sizes to standardize MTBE removal adsorption efficiency with surface-modified kaolin serving as the adsorbent, this technique was employed to optimize the ideal column size (Kiadehi *et al.*, 2017). The adsorbent substance was activated by the thermal temperature (Dong *et al.*, 2017). The goal of this study was to characterize Kaolin adsorbents using XRD, SEM, and FTIR, to demonstrate surface changes in the adsorbent following reaction with KOH, and after adsorption study the morphological changes were determined by surface characterization and comparison of adsorption properties of different surface modified Kaolin (Ma *et al.*, 2017) to clarify the adsorption mechanism and assess the effects of pore structure and surface chemistry of adsorbents on the adsorption (Songsiri *et al.*, 2017). Thomas and Thomson models were used to determine the adsorption isotherms and kinetics (Grieco *et al.*, 2017). This work argued that rate driving forces follow second-order reversible reaction kinetics and that there is no axial dispersion based on the premise of adsorption-desorption (Abbas *et al.*, 2017). This paper talks about the regeneration of the column. To determine the surface-modified column's capacity for reuse, a chemical regeneration method and adsorption using recycled adsorbent were used.

2. Methodology

2.1. Adsorbent preparation

Using potassium nitrate hexahydrate, commercial kaolin from Sigma Aldrich was employed as an adsorbent before being impregnated with KOH at various loading percentages (2, 4, 6, and 10%) (Gao *et al.*, 2017). After distillation in a Lab Strong Fil Streem II 4S Glass Still distiller Filstreem, an equivalent amount of potassium precursor was dissolved in de-ionized water (20 mS/cm) from Thermo Scientific's Barnstead NANOPURE setup to create the impregnation solution (Konggidinata *et al.*, 2017). For the purpose of dispersing potassium nitrate, the Kaolin with KOH-impregnating solution was allowed to dry gradually at 100^{o}C for 10 hours (Xie *et al.*, 2016). After calcination at 990^{o}C for 250 minutes with a steady supply of high quality (98.999%) H_2 gas, the final adsorbent was produced (Metcalf *et al.*, 2016). Kaolin-KOH(x), where x is the theoretical weight percent of KOH contained on the matrix, is the naming scheme that has been used (Lin *et al.*, 2020). For instance, Kaolin-KOH denotes a sample that contains 6% KOH while pure Kaolin is the untagged sample.

2.2. Concentrated MTBE solution preparation

MTBE (99.9%) was supplied by Sigma. Deionized water or methanol (HPLC grade) were utilized to make the solutions (Jiang *et al.*, 2020). HCL acid was used as a supporting electrolyte. HPLC grade (98%) was used in the liquid-liquid extraction. Solutions containing 1000 mg L^{-1} of MTBE in methanol and water medium containing 500 mmol L^{-1} of electrolyte (H_2SO_4) were made in order to test the efficacy of the contaminant removal (Yin *et al.*, 2020). The prepared concentrated MTBE solution had a concentration of 10.00 mg/L.

2.3. HPLC techniques

Sigma Co and AR Grade provided the MTBE standard, which was bought. Solvents of HPLC quality were purchased from Alikanj (Lucknow, India) (Dubuis *et al.*, 2019). Other chemical reagents, which were bought from nearby vendors, are of the analytical or biochemical quality. The standard substance was dissolved in 50% ethanol to create MTBE stock solution (10 mg mL1), which was then kept at 50°C (Liu *et al.*, 2019). For the creation of the MTBE standard curve, the stock solution was diluted to various concentrations ranging from 1.0 to 10g mL1 using 50% ethanol (Huang *et al.*, 2019). 40% ethanol was used as the washing solvent, and pH levels of 2.5 and 3.5 were achieved by adding 2 MHCl to the loading solvent (Mejia *et al.*, 2020). The eluting solvent was 90% ethanol adjusted with 2 M NaOH to pH 12.

2.4. Adsorption study

For the fixed bed column investigations, a glass column with an inner diameter of 4 cm and a length of 80 cm was used (de la Luz *et al.*, 2020). The particle sizes of the Kaolin-KOH utilized had a starting point of 0.5mm. The column was filled with kaolin-KOH, and the bottom was covered with sponge wool (Pongkua *et al.*, 2020). There were beds with heights of 12, 8, and 4 cm. The used flow rates varied from 4 to 10 mL/min (Yang *et al.*, 2020). The residual MTBE level in the effluent samples was estimated by IC after samples were taken at regular intervals (Julien *et al.*, 2020). When the column started to tire, the inquiries into it were over (Nicholls *et al.*, 2020). For practical reasons, the column studies are conducted at room temperature.

2.5. Characterization by XRD, SEM and FTIR

A Cu-K (= 0.14857 nm) radiation source was used with an X-ray diffractometer (PANalytical, 28 X'Pert PRO) to accomplish the XRD measurements (Liu *et al.*, 2018). The source's voltage and current were measured to be 60 kV and 80 mA, respectively, for the 3 scan XRD data obtained in continuous scan mode at a scanning speed of 7°/min (Yu *et al.*, 2019). After the samples were outgassed for 8 hours at 110°C, a H_2 adsorption-desorption isotherm was determined at 88K using a surface area and pore size analyser (Yu *et al.*, 2017). The morphology was examined using a field emission scanning electron microscope, and the chemical compositions were examined using the scanning electron microscopes FDX detector (Abdelrasoul *et al.*, 2017). The TG-DTG-DTAs were performed using a thermal determiner by applying a heating rate of 30.0 °C/min up to 1600 °C in an air environment (Qian *et al.*, 2018). Using an FTIR analyser and the FBr matrix approach, the FTIR spectra were collected over the spectrum range of 6000 cm^{-1} to 600 cm^{-1} (Gorityala *et al.*, 2018). Captivating extents were performed at optimum heat using and a maximum magnetic field (Wang *et al.*, 2020).

2.6. Kinetic study

2.6.1. Thomas model

The link between solute concentration and time was calculated using the Thomas model. Both internal and external mass transfer constraints were considered in continuous column technology (Abdellatief *et al.*, 2020).

$$\ln\left(\frac{Co}{Ct}-1\right)=(\mathrm{Kt}*q*m/Q)-kt*Co*t$$

where K_t is the Thomas rate constant (in mL/(min.mg), Co and Ct are the influent and effluent concentrations, respectively, in mg/L, and t is the period (min), The amount of adsorbent in the column, Q (g), was calculated using a constant flow rate, and the adsorption kinetics (k_t) were calculated from the plot of ln [(co/ct)] over time (Karmakar and Halder, 2019). The Thomas model is represented by the ranges of regression coefficients.

2.6.2. Thomson model

The link between internal and external adsorption processes was discovered using the Thomson model. Equation can be used to express the Thomson model.

$$ln\left(\frac{Co}{Ct}-1\right)=\frac{kTH\ qeW\ -\ kTH\ Co\ t}{Q}$$

kTH is the Thomson rate constant (ml/min.mg), where qe is the adsorption capacity, Co is the inlet ion concentration, Ct is the effluent ion concentration at time t (mg/L), W is the mass of the adsorbent (g), Q is the inlet flow rate (ml/min), and t is the flow time t. (min) (Wang *et al.*, 2019). The value of Co/Ct is the ratio of the ion concentrations at the intake and outflow. Squeezing ln (Co/Ct-1) against time yielded the values of qe and kTH from the interception point and slope of the plot, respectively (t).

2.6.3. Intraparticle diffusion model

The Weber-Morris intraparticle diffusion model was used. The following equation served as the introduction to this model:

$q_t=K_{id}t^{0.5}+C$

K_{id} stands for the intraparticle diffusion model's rate constant (mgr/gr.min0.5), and C is a constant (mgr/gr) (Lu *et al.*, 2017). The values of Kid and C can be calculated from the linear relationship between the values of qt and t0.5.

3. Result and discussion

3.1. Adsorption study

To determine how well Kaolin-KOH served as an adsorbent for the removal of MTBE, batch process research was used to analyse MTBE adsorption. For the MTBE removal research, a sample was taken every five minutes, and gas chromatography was utilized to determine how well the treatment was working. Investigations were conducted on the first round of therapy study using Kaolin-KOH columns. The input sample level was 4 mL/min in a 12 cm column, whereas the output ranges were 0.4 mL/min. The therapeutic efficacy within the first hour varied between 10mg/L (Zhao *et al.*, 2016). The column was totally depleted in the region of 0.55mg/l for 12 cm in 90 minutes which was clearly mentioned in Table 1 & Figure 1.

Table 1. MTBE removal study by 12cm column

Time (min)	12cm column (mg/L)
0	10
5	8.13
10	7.94
15	7.61
20	6.86
25	6.32
30	5.94
35	5.91
40	4.75
45	4.20
50	3.87
55	2.94
60	2.13
65	1.74
70	1.18
75	0.93
80	0.74
85	0.55
90	0.55

The effectiveness of Kaolin-KOH as an adsorbent for the elimination of MTBE was examined using batch process study. Gas chromatography was used to assess the efficacy of the therapy in the MTBE elimination investigation after samples were taken every five minutes. Investigations on the initial therapeutic research utilizing Kaolin-KOH columns were done (He *et al.*, 2021). The output ranges were kept at 0.4 mL/min while the input

sample level was 4 mL/min in an 8 cm column. Within the first hour, the therapeutic effectiveness ranged between 10mg/L. In 80 minutes, the column was completely

depleted at a concentration of around 0.62 mg/l for 8 cm. It is proved by Table 2 and in Figure 2.

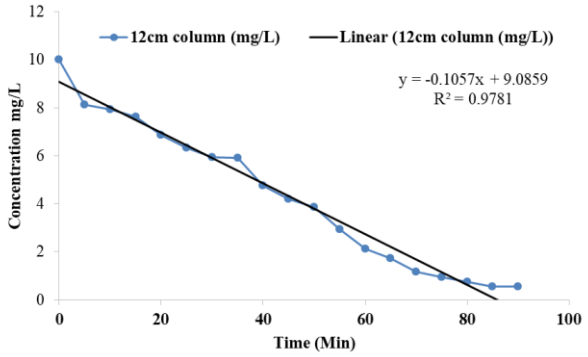

Figure 1. MTBE removal by 12cm column

Table 2. MTBE removal study by 8cm column

Time (min)	8cm column (mg/L)
0	10
5	9.78
10	8.91
15	8.33
20	7.84
25	7.12
30	6.73
35	6.01
40	5.62
45	4.97
50	4.21
55	3.65
60	2.32
65	1.94
70	0.91
75	0.62
80	0.62

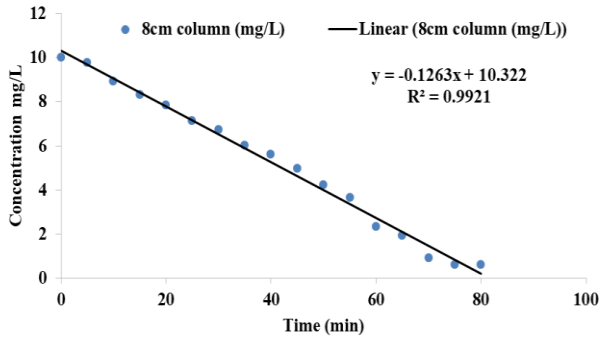

Figure 2. MTBE removal by 8cm column

Using a batch process investigation, the efficacy of Kaolin-KOH as an adsorbent for the removal of MTBE was evaluated. After samples were taken every five minutes, gas chromatography was employed to evaluate the therapy in the MTBE elimination experiment. Investigations on the first Kaolin-KOH column-based therapeutic study were conducted (Jia *et al.*, 2021). The input sample level was 4 mL/min in a 4 cm column, and the output ranges were maintained at 0.4 mL/min (Roumiguieres *et al.*, 2018). The therapeutic effectiveness peaked at 10 mg/L within the first hour. The column was totally drained in 75 minutes at a concentration of roughly 0.91 mg/l for 4 cm. In Table 3 and Figure 3, it is stated quite clearly.

Table 3. MTBE removal study by 4cm column

Time (min)	4cm column (mg/L)
0	10
5	9.32
10	9.10
15	8.81
20	7.92
25	7.61
30	6.75
35	6.10
40	5.84
45	4.73
50	4.13
55	3.96
60	3.31
65	1.99
70	0.91
75	0.91

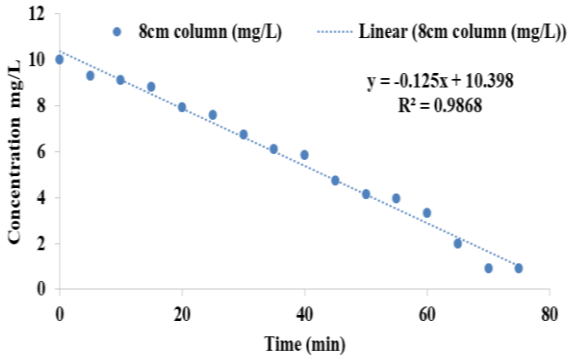

Figure 3. MTBE removal by 4cm column

3.2. HPLC chromatogram analysis

Following the adsorption study, the samples were collected and placed in vials that were kept in the refrigerator to view the chromatogram. A 10 µl sample was injected into the intake region and run through the mobile phase and stationary phase while the optimal level was calculated using the gas chromatography result graph. Following software analysis of the graphical depiction, MTBE was measured using HPLC (Pezzotta *et al.*, 2018). Based on the graphical representation, the sample's MTBE content was calculated using the peak's height and area. According to the HPLC graph, which is illustrated by Figure 4, MTBE achieved better clearance than other substances.

3.3. Characterization

3.3.1. XRD study

The XRD patterns of surface modified Kaolin-KOH and the samples synthesized under various circumstances are shown in Figure 5. Based on the XRD pattern, chemical makeup, and manufacturing method, it can be established that the main mineral components of kaolinite-type pyrite cinder are amorphous nature and magnetite coupling, the minor of hematite, and a trace of anatase. Only weak diffusion peaks of Kaolin are shown in the experiments synthesized at 60°C, which may be the extra crystal seed, although no zeolite quartz segment is apparent. As a result, 55°C is insufficient for the synthesis of kaolinite. The outcomes show that Kaolin-KOH can be produced at 60 °C. Kaolin crystallization is aided by the complicated heat, but quartz development must last for at least 4 hours and no longer than 10 hours to prevent the formation of sodalite (Rose *et al.*, 2021). According to an analysis of the XRD Figure 5, the two key factors in the synthesis of the Kaolin-KOH adsorbent are the crystallization temperature and the crystallization time.

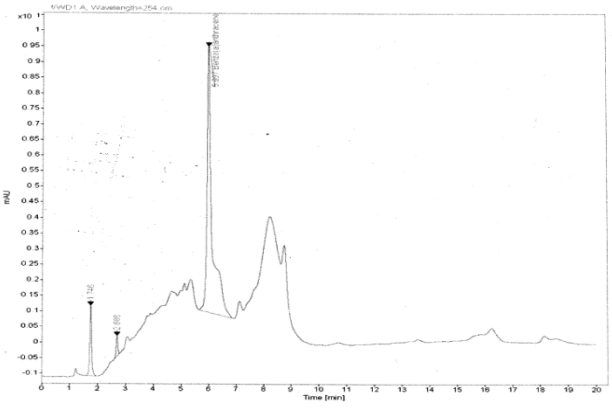

Figure 4. HPLC sample chromatogram of MTBE removal study

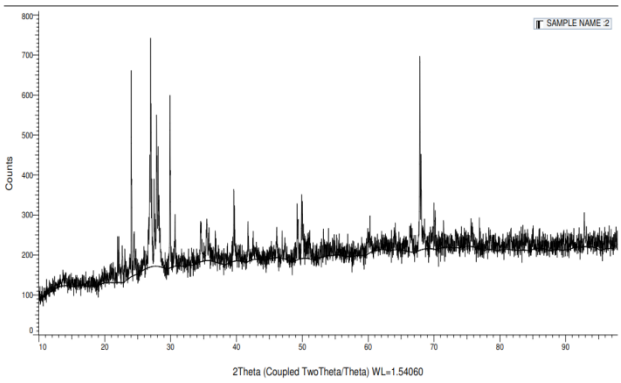

Figure 5. XRD Pattern for Kaolin-KOH adsorbent

3.3.2. SEM analysis

It is discovered that the SEM analysis and the Kaolin + KOH have a good association. Additionally, the SEM demonstrated that the high quantization of kaolin is raised, at this is significantly condensed by the sample contains the quartz type of structure. The ideal hydrothermal synthesis conditions are 10g KOH, 5 g NaOH, 50 ml H_2O, 90 °C crystallization temperature, and 10 h crystallisation time, according to a thorough investigation of the results of XRD and SEM. The magnetic Kaolin synthesized with KOH is shown in the SEM. Figure 6 depicts the Kaolin-KOH adsorbent's adsorption-desorption isotherms, The insets display a closer look at how the smaller and larger particles spread throughout the aperture. Gurvich's rule states that the total hole capacity is 1.1245 cm^3/g and that the apertures are less than 465.2 nm. According to the SF method, the tiny volume fluctuations are 1.009 cm^3/g, the microstructure ranges from 0.6 to 6.7 nm, and the corresponding magnitude is 1.482 nm (Ridwan *et al.*, 2021). According to the BJH model, the corresponding size is 5.419 nm, the structural change's magnitude ranges from 2.9 to 194.6 nm, and the mesopore volume is 0.08 cm^3/g.

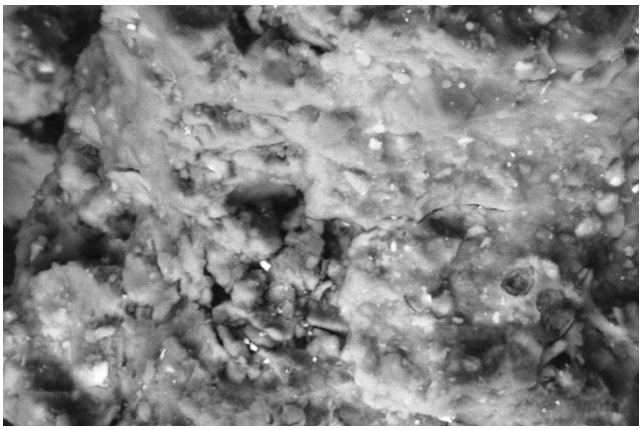

Figure 6. SEM Analysis of Kaolin-KOH adsorbent

3.3.3. FTIR analysis

The FTIR spectra of the synthetic Kaolin-KOH adsorbent is shown in Figure 7. The spectra showed all the kaolin-related adsorption bands. The crews at 587 cm^{-1}, 674 cm^{-1}, and 1124 cm^{-1} are responsible for the atmospheres of the K-O winding, dual sphere twisting, and uneven bounce KOH, respectively. Interstitial bonded water and intra- and intermolecular hydrogen bonding, respectively, are related by the bands at 6000-6900 cm^{-1} and 1860 cm^{-1}. junctions with the kaolin crew at 674 cm^{-1} and the crew for the magnetite that needs to be distributed at 668 cm^{-1}. This observation is consistent with the description of an intriguing kaolin synthesis that is analogous. The results of the FTIR investigation show that neither the crystal structure nor the synthesis of kaolin-KOH are affected by the presence of attracting particles (He *et al.*, 2019).

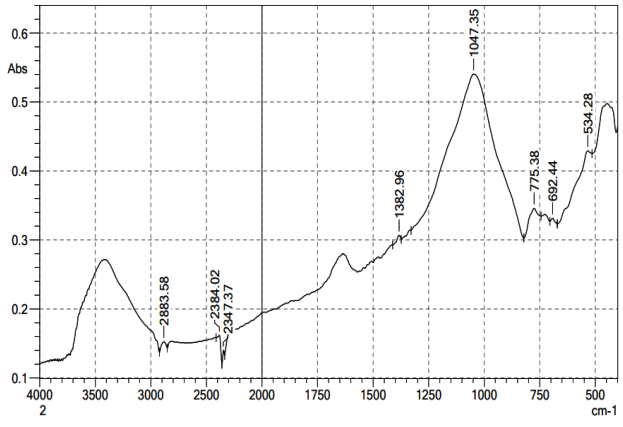

Figure 7. FTIR Analysis of Kaolin-KOH adsorbent

3.4. Kinetic study

3.4.1. Thomas model

The ionic speciation of the adsorbate that was present at the binding site controlled the adsorption process. The examination made use of the Thomas model. Both the measured adsorption process and the anticipated break through curve were consistent. The value of k_t is dependent on the mass (m) and time of concentration, and the regression coefficient for 0.09781 (R^2) (t). The lowest k_t value at the highest Co demonstrates that the adsorption kinetics were favourable at the highest adsorbate concentration. Initial k_t values were lower; at the next level, they rose to 0.0945 for a 12 cm column, 0.0982 for an 8 cm column, and 0.0912 for a 4 cm column. The rate constant (k_t) fluctuated as the bed depth increased. The equilibrium uptake capacity (q_o), which was 46.00 for 12 cm, 58.70 for 8 cm, and 18.93 for 4 cm, increased slightly, as indicated in Table 4. The decline in q_o demonstrated that there is an inverse relationship between bed height, contact time, and adsorption capacity. decreased influent concentration and flow rate, whereas higher bed heights speed up adsorption (Bunmahotama *et al.*, 2017). The triangular connection of the adsorption rate constant was shown in Figure 8.

Table 4. Thomas model for Three different sized column

Column size (cm)	k_t x 10^{-3} (mL/(min.mg)	q_o (mg/g)	R^2
12	0.0945	46.00	0.9781
8	0.0982	58.70	0.9921
4	0.0912	18.93	0.9868

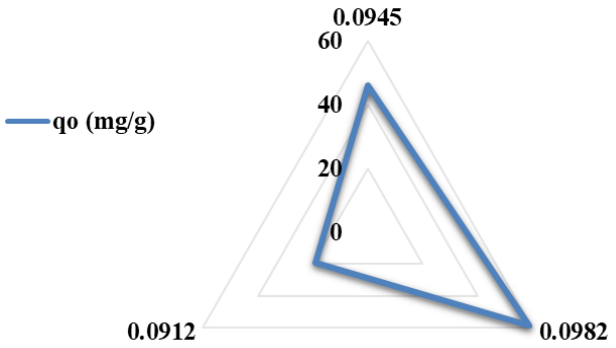

Figure 8. Thomas Model Triangle scattering

3.4.2. Thomson Model

The results of the experimental investigation were strong candidates for the Thomson model. The inflow concentration (Co) was seen to be consistently maintained in the 4ml/min range. The kTH also changed as a result of the Thomson rate constant. The height of the bed also had an impact on how the kTH value changed. The kTH dropped from 53.13 mL/min. mg for a 12 cm column, 62.48 mL/min. mg for an 8 cm column, and 39.74 mL/min. mg for a 4 cm column. The stronger driving power of the inflow concentration may be the reason for this, as evidenced by the fact that the qe rose for distances of 12 cm (0.0847 mg/g), 8 cm (0.0912 mg/g), and 4 cm (0.0901 mg/g). R^2 for columns of 12 cm, 8 cm, and 4 cm, respectively, was 0.9641, 0.9733, and 0.9714 (Li *et al.*, 2020). Adsorption rate constant triangular linkage is shown in Figure 9.

Table 5. Thomson model for Three different sized column

Column size (cm)	qe (mg/g)	k_{TH} (mL/min.mg)	R^2
12	0.0847	53.13	0.9641
8	0.0912	62.48	0.9733
4	0.0901	39.74	0.9714

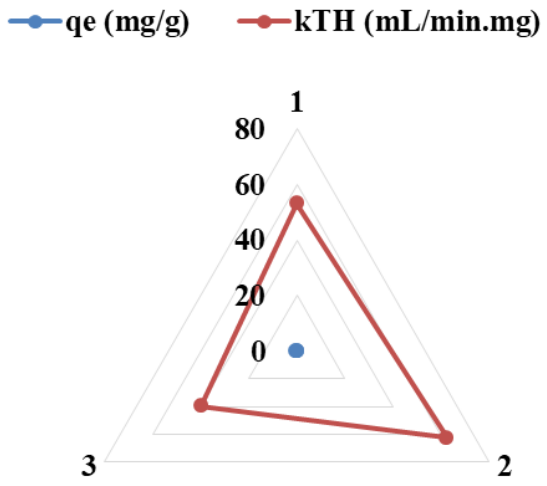

Figure 9. Thomson Model Triangle scattering

3.4.3. Intra particle diffusion model

To explain experimental data, intraparticle diffusion has been examined as a kinetic model. This kinetic model is thought to be the best representation of the adsorption of Kaolin-KOH isomers based on the high regression coefficient (96% - 99%) shown in Table 6. In comparison to other isomers, MTBE had a higher removal rate and adsorption loading. In certain circumstances, the presence of methyl groups may facilitate quicker clearance (Stefanakis *et al.*, 2016). The intraparticle diffusion models provided in Table 6 have low R^2 values, which means that these models are inadequate for interpreting experimental results.

Table 6. Intra particle diffusion of Adsorption study

Column size (cm)	qe/C	K1/K2/Kdif.	R^2
12	1.4517	-0.0064	0.9821
8	7.3879	-0.0532	0.9996
4	8.0621	-0.0274	0.9626

4. Conclusion

The effectiveness of the surface modified Kaolin with KOH adsorbent doped with different column heights was tested for its ability to adsorb MTBE from aqueous phase. Due to its enhanced surface characteristics and negligible surface area compromise, the adsorbent exhibits good performance. The prepared columns of 12 cm, 8 cm, and 4 cm had removal efficiencies of about 97.79, 99.08, and 98.13 respectively. This study established that the ideal column size for this experiment was 8 cm, as indicated by the Thomas model and Thomson model, which

established a correlation of R^2 of 97.81, 99.21, and 98.36 respectively. The high regression coefficient (96%–99%) indicated the isomers in the intraparticle diffusion. The surface morphological changes after the treatment process were shown by XRD, SEM, and FTIR in the characterisation investigation. It displayed a balance of surface properties that allowed for improved interaction between the molecules and particles of the adsorbate, and this interaction made it easier to remove the MTBE adsorbate. Through parametric dosage, contact time, and concentration tests, the adsorption process was also examined. According to the obtained data, the high MTBE adsorption capability in comparison to other Kaolin-KOH adsorbents suggests its potential use in adsorption studies.

Conflict of Interest

The authors declare no conflict of interest.

Acknowledgement

The authors are grateful to GMR Institute of Technology, Rajam Andhra Pradesh for providing facilities for the conduct of laboratory Investigations. The authors extend their appreciation to the Researchers Supporting Project number (RSP2023R396), King Saud University, Riyadh, Saudi Arabia.

References

Abbas A., Sallam A.S., Usman A.R.A. and Al-Wabel M.I. (2017). Organoclay-based nanoparticles from montmorillonite and natural clay deposits: Synthesis, characteristics, and application for MTBE removal. *Applied Clay Science*, **142**, 21–29.

Abdellatief T.M.M., Ershov M.A. and Kapustin V.M. (2020). New recipes for producing a high-octane gasoline based on naphtha from natural gas condensate. *Fuel*, **276**, 118075.

Abdelrasoul A., Zhang H., Cheng C.H.. and Doan H. (2017). Applications of molecular simulations for separation and adsorption in zeolites. *Microporous and Mesoporous Materials*, **242**, 294–348.

Amanollahi H., Moussavi G. and Giannakis S. (2019). VUV/Fe(II)/H_2O_2 as a novel integrated process for advanced oxidation of methyl tert-butyl ether (MTBE) in water at neutral pH: Process intensification and mechanistic aspects. *Water Research*, **166**, 115061.

Attarian P. and Mokhtarani N. (2021). Comparison of co-metabolic and direct metabolic biodegradation of MTBE: Monitoring main intermediates and SBR stable operation. Environmental Technology and Innovation, 22, 101475.

Attarian P. and Mokhtarani N. (2021). Feasibility study of aerobic cometabolism biodegradation of MTBE by a microbial consortium: Biomass growth and decay rate. *Journal of water processing engineering*, **44**, 102338.

Bunmahotama W., Hung W.N. and Lin T.F. (2017). Prediction of the adsorption capacities for four typical organic pollutants on activated carbons in natural waters. *Water Research*, **111**, 28–40.

de la Luz A.P., luga C. and Vivier-Bunge A. (2020). An effective force field to reproduce the solubility of MTBE in water. *Fuel*, **264**, 116761.

Dong C.D., Tsai M.L., Chen C.W. and Hung C.M. (2017). Heterogeneous persulfate oxidation of BTEX and MTBE using Fe_3O_4−CB magnetite composites and the cytotoxicity of degradation products. *International Biodeterioration & Biodegradation*, **124**, 109–118.

Dubuis A., Masle A.L., Chahen L., Destandau E. and Charon N. (2019). Centrifugal partition chromatography as a fractionation tool for the analysis of lignocellulosic biomass products by liquid chromatography coupled to mass spectrometry. *Journal of Chromatography A*, **1597**, 159–166.

Gao R., Zhang Q., Lv R., Soyekwo F., Zhu A. and Liu Q. (2017). Highly efficient polymer–MOF nanocomposite membrane for pervaporation separation of water/methanol/MTBE ternary mixture. *Chemical Engineering Research and Design*, **117**, 688–697.

Gong T., Zhang X., Li Y. and Xian Q. (2016). Formation and toxicity of halogenated disinfection byproducts resulting from linear alkylbenzene sulfonates. *Chemosphere*, **149**, 70–75.

Gorityala S., Yang S., Montano M.M. and Xu Y. (2018). Simultaneous determination of dihydrotestosterone and its metabolites in mouse sera by LC-MS/MS with chemical derivatization. *Journal of Chromatography B*, **1090**, 22–35.

Grieco S.A., Ramarao B.V., Schulte J. and Kiemle D. (2017). Adsorption equilibrium and mechanisms of tris(2-chloroethyl)phosphate (TCEP) on zeolite-β under environmentally relevant and competitive conditions with methyl tert-butyl ether (MTBE). *Environmental Technology and Innovation*, **8**, 172–181.

He K.Y., Wei Q., Wang Y.L., Wang S., Cui S.P., Li Q.Y. and Nie Z.R. (2019). Hydrophobic mesoporous organosilicon membranes: Preparation and application in the separation of volatile organic compounds from water. *Microporous and Mesoporous Materials*, **288**,109606.

He Z., Liu Z. and Gong L. (2021). Systematic evaluation of sample preparation strategy for GC-MS-based plasma metabolomics and its application in osteoarthritis. *Analytical Biochemistry*, **621**, 114153.

Huang Y., Li W., Qin L., Xie X., Gao B., Sun J. and Li A. (2019). Distribution of endocrine-disrupting chemicals in colloidal and soluble phases in municipal secondary effluents and their removal by different advanced treatment processes. *Chemosphere*, **219**, 730–739.

Jia B., Jiang X., Chen X. and Dong S. (2021). Experimental determination and modeling of liquid-liquid equilibrium for ternary mixtures composed of water, epichlorohydrin and different solvents. *Journal of molecular Liquids*, **322**, 114984.

Jiang N., Shang R., Heijman S.G.J. and Rietveld L.C. (2018). High-silica zeolites for adsorption of organic micro-pollutants in water treatment: A review. *Water Research*, **144**, 145–161.

Jiang N., Shang R., Heijman S.G.J. and Rietveld L.C. (2020). Adsorption of triclosan, trichlorophenol and phenol by high-silica zeolites: Adsorption efficiencies and mechanisms. *Separation and Purification Technology*, **235**, 116152.

Julien M., Gori D., Hohener P., Robin R.J. and Remaud G.S. (2020). Intramolecular isotope effects during permanganate oxidation and acid hydrolysis of methyl tert-butyl ether. *Chemosphere*, **248**, 125975.

Karmakar B. and Halder G. (2019). Progress and future of biodiesel synthesis: Advancements in oil extraction and conversion technologies. *Energy Conversion and Management*, **182**, 307–339.

Kiadehi A.D., Edabi A. and Aghaeinejad-Meybodi A. (2017). Removal of methyl tert-butyl ether (MTBE) from aqueous medium in the presence of nano-perfluorooctyl alumina (PFOAL): Experimental study of adsorption and catalytic ozonation processes. *Separation and Purification Technology*, **182**, 238–246.

Konggidinata M.I., Chao B., Lian Q., Subramaniam R., Zappi M. and Gang D.D. (2017). Equilibrium, kinetic and thermodynamic studies for adsorption of BTEX onto Ordered Mesoporous Carbon (OMC). *Journal of Hazardous Materials*, **336**, 249–259.

Li Q., Fan W., Yan H., Huang X., Zhang L. and Ma Z. (2020). Experimental determination and modeling of liquid-liquid equilibrium for water + diethoxymethane + methyl tert-butyl ether (or methyl isobutyl ketone) at 298.15, 308.15, and 318.15 K. *Fluid Phase Equilibria*, **505**, 112353.

Lin C.C., yan G.W., Cheng Y.H. and Shie R.H. (2020). Exposure levels of volatile organic compounds and potential health risks for passengers and workers at an intercity bus terminal. *Atmospheric Pollution Research*, **11**, 1820–1828.

Liu C., Chen D.W., Ren Y.Y. and Chen W. (2019). Removal efficiency and mechanism of phycocyanin in water by zero-valent iron. *Chemosphere*, **218**, 402–411.

Liu X., Yi D., Cui Y., Shi L. and Meng X. (2018). Adsorption desulfurization and weak competitive behavior from 1-hexene over cesium-exchanged Y zeolites (CsY). *Journal of Energy Chemistry*, **27**, 271–277.

Lu Q., Toledo R.A., Xie F., Li J. and Shim H. (2017). Reutilization of waste scrap tyre as the immobilization matrix for the enhanced bioremoval of a monoaromatic hydrocarbons, methyl tert-butyl ether, and chlorinated ethenes mixture from water. *Science of the total removal*, **583**, 88–96.

Ma C., Liu H., Qiu J. and Zhang X. (2021). Bimetallic Zn/Co-ZIF tubular membrane for highly efficient pervaporation separation of Methanol/MTBE mixture. *Journal of membrane science,* **638**, 119676.

Ma J., Xiong D., Li H., Ding Y., Xia X.C. and Yang Y. (2017). Vapor intrusion risk of fuel ether oxygenates methyl tert-butyl ether (MTBE), tert-amyl methyl ether (TAME) and ethyl tert-butyl ether (ETBE): A modeling study. *Journal of Hazardous Materials*, **332**, 10–18.

Masle A.L., Santin S., Marlot L., Chahen L. and Charon N. (2018). Centrifugal partition chromatography a first dimension for biomass fast pyrolysis oil analysis. Analytica Chimica Acta, **1029**, 116–124.

Mejia A., Cartes M. and Chaparro G. (2020). Isobaric vapor – liquid – liquid equilibrium for water + MTBE + alcohol (ethanol or 1-butanol) mixtures. *Fluid Phase Equilibria*, **523**, 112768.

Metcalf M.J., Stevens G.J. and Robbins G.A. (2016). Application of first order kinetics to characterize MTBE natural attenuation in groundwater. *Journal of contaminant hydrology*, **187**, 47–54.

Muller A., Becker R., Dorgerloh U., Simon F.G. and Braun U. (2018). The effect of polymer aging on the uptake of fuel aromatics and ethers by microplastics. *Environmental Pollution*. **240**, 639–646.

Nicholls H.C.G., Mallinson H.E., Rolfe S.A., Hjort M., Spence M.J. and Thornton S.F. (2020). Influence of contaminant exposure on the development of aerobic ETBE biodegradation potential in microbial communities from a gasoline-impacted aquifer. *Journal of Hazardous Materials*, **388**, 122022.

Park K.Y., Yu Y.J., Yun S.J. and Kweon J.H. (2019). Natural organic matter removal from algal-rich water and disinfection by-products formation potential reduction by powdered activated carbon adsorption. *Journal of Environmental Management*, **235**, 310–318.

Pezzotta C., Fleury G., Soetens M., Vander Perre S., Denayer J.F.M., Riant O. and Gaigneaux E.M. (2018). Improving the selectivity to 4-tert-butylresorcinol by adjusting the surface chemistry of heteropolyacid-based alkylation catalysts. *Journal of catalysis*, **359**, 198–211.

Pongkua W., Dolphen R. and Thiravetyan P. (2020). Bioremediation of gaseous methyl tert-butyl ether by combination of sulfuric acid modified bagasse activated carbon-bone biochar beads and Acinetobacter indicus screened from petroleum contaminated soil. *Chemosphere*, **239**, 124724.

Qian H., Lin Y.L., Xu B., Wang L.P., Gao Z.C. and Gao N.Y. (2018). Adsorption of haloforms onto GACs: Effects of adsorbent properties and adsorption mechanisms. *Chemical Engineering Journal*, **349**, 849–859.

Ren Q., Xie X., Tang Y., Hu Q. and Du Y. (2021). Methyl tertiary-butyl ether inhibits THP-1 macrophage cholesterol efflux in vitro and accelerates atherosclerosis in ApoE-deficient mice in vivo. *Journal of Environmental Science*, **101**, 236–247.

Ridwan I., Chinwanitcharoen C. and Tamura K. (2021). A new biodiesel production by water addition to supercritical tert-butyl methyl ether using a plug flow reactor. Fuel, 305, 121512.

Rose A., Jaczynski J. and Matak K. (2021). Extraction of lipids from insect powders using a one-step organic solvent extraction process. *Future Foods*, **4**, 100073.

Roumiguieres A., Kinani A., Bouchonnet S. and Kinani S. (2018). Development and validation of a multiclass method for the determination of organohalogen disinfectant by-products in water samples using solid phase extraction and gas chromatography-tandem mass spectrometry. *Journal of Chromatography B*, **1579**, 89–98.

Songsiri N., Rempel G.L. and Kich P.P. (2017). Liquid-phase synthesis of isoprene from MTBE and formalin using cesium salts of silicotungstic acid. *Molecular catalyst*, **439**, 41–49.

Stefanakis A.I., Seeger E., Dorer C., Sinke A. and Thullner M. (2016). Performance of pilot-scale horizontal subsurface flow constructed wetlands treating groundwater contaminated with phenols and petroleum derivatives. *Ecological Engineering*, **95**, 514–526.

Wang J., Wang Z., Vieira C.L.Z., Wolfson J.M. and Pingtian G., Huang S. (2019). Review on the treatment of organic pollutants in water by ultrasonic technology. *Ultrasonic Sonochemistry*, **55**, 273–278.

Wang Y., Zhao M. and Liu T. (2020). Extraction of allelochemicals from poplar alkaline peroxide mechanical pulping effluents and their allelopathic effects on Microcystis aeruginosa. *Journal of Bioresource and Bioproducts*, **5**, 276–282.

Xie F., Lu Q., Toledo R.A. and Shim H. (2016). Enhanced simultaneous removal of MTBE and TCE mixture by Paracoccus sp. immobilized on waste silica gel. *International Biodeterioration and Biodegradation*, **114**, 222–227.

Yang C., Miao G., Pi Y., Xia Q., Wu J., Li Z. and Xiao J. (2019). Abatement of various types of VOCs by adsorption/catalytic oxidation: A review. *Chemical Engineering Journal*, **370**, 1128–1153.

Yang Q., Shao S., Zhang Y., Hou H., Qin C., Sun D. and Liu Y. (2020). Comparative study on life cycle assessment of gasoline with methyl tertiary-butyl ether and ethanol as additives. *Science of the total environment*, **724**, 138130.

Yin T., Wu Y., Shi P., Li A., Xu B., Chu W., Pan Y. (2020). Anion-exchange resin adsorption followed by electrolysis: A new disinfection approach to control halogenated disinfection byproducts in drinking water. *Water Research*, **168**, 115144.

Yu X., Liu H., Diao J., Sun Y. and Wang Y. (2019). Magnetic molecularly imprinted polymer nanoparticles for separating aromatic amines from azo dyes – Synthesis, characterization, and application. *Separation and Purification Technology*, **204**, 213–219.

Yu Z., Meng X., Liu N. and Shi L. (2017). A novel disposal approach of deactivated resin catalyst for methyl tert-butyl ether synthesis: Preparation of low-cost activated carbons with remarkable performance on dibenzothiophene adsorption, *Fuel*, **207**, 47–55.

Yunhui Z., jin F., Shen Z., Lynch R. and Al-Tabbaa A. (2018). Kinetic and equilibrium modelling of MTBE (methyl tert-butyl ether) adsorption on ZSM-5 zeolite: Batch and column studies. *Journal of Hazardous Materials*, **347**, 461–469.

Zhang Y., Jin F., Shen Z., Wang F., Lynch R. and Al-Tabbaa A. (2019). Adsorption of methyl tert-butyl ether (MTBE) onto ZSM-5 zeolite: Fixed-bed column tests, breakthrough curve modelling and regeneration. *Chemosphere*, **220**, 422–431.

Zhao Y.W., Shen B., Sun H., Zhan G.X. and Liu J.C. (2016). Adsorption of dimethyl disulfide on ZSM-5 from methyl tert-butyl ether liquid: A study on equilibrium and kinetics. *Fuel Processing Technology*, **155**, 14–19.

Zhi Y. and Liu J. (2016). Surface modification of activated carbon for enhanced adsorption of perfluoroalkyl acids from aqueous solutions. *Chemosphere*, **144**, 1224–1232.